SYNTHETIC BIOLOGY

Transistor in a tube: A route to three-dimensional bioelectronics

C. Pitsalidis[1]*, M. P. Ferro[2], D. Iandolo[1], L. Tzounis[3], S. Inal[4], R. M. Owens[1]*

Advances in three-dimensional (3D) cell culture materials and techniques, which more accurately mimic in vivo systems to study biological phenomena, have fostered the development of organ and tissue models. While sophisticated 3D tissues can be generated, technology that can accurately assess the functionality of these complex models in a high-throughput and dynamic manner is not well adapted. Here, we present an organic bioelectronic device based on a conducting polymer scaffold integrated into an electrochemical transistor configuration. This platform supports the dual purpose of enabling 3D cell culture growth and real-time monitoring of the adhesion and growth of cells. We have adapted our system to a 3D tubular geometry facilitating free flow of nutrients, given its relevance in a variety of biological tissues (e.g., vascular, gastrointestinal, and kidney) and processes (e.g., blood flow). This biomimetic transistor in a tube does not require photolithography methods for preparation, allowing facile adaptation to the purpose. We demonstrate that epithelial and fibroblast cells grow readily and form tissue-like architectures within the conducting polymer scaffold that constitutes the channel of the transistor. The process of tissue formation inside the conducting polymer channel gradually modulates the transistor characteristics. Correlating the real-time changes in the steady-state characteristics of the transistor with the growth of the cultured tissue, we extract valuable insights regarding the transients of tissue formation. Our biomimetic platform enabling label-free, dynamic, and in situ measurements illustrates the potential for real-time monitoring of 3D cell culture and compatibility for use in long-term organ-on-chip platforms.

INTRODUCTION

Cell-based assays have been extensively used for drug discovery as well for understanding molecular mechanisms of disease for several decades. Although the majority of techniques rely on optical transducers, electrical transduction is arguably a hugely data-rich and dynamic means of interfacing with cells. Most electrical measurements have so far focused on electrophysiological interfacing with electrogenic cells (e.g., neurons or cardiac tissues) (*1*, *2*). However, a substantial body of work exists using electrical impedance methods to monitor properties of cells as diverse as adhesion to micromotion in a noninvasive, label-free manner, owing to the pioneering work of Giaever and Keese (*3*). Transistors, thought by many to be a revolutionary invention that enabled the era of microelectronics, can be used as transducers of biological signals when integrated with electrolytes (*4*). As an electrolyte-gated transistor, organic electrochemical transistors (OECTs) have been particularly favored for biotransduction as they can transduce biological signals into electrical output using very low operation voltages (*5*). The OECT uses an organic semiconductor film in the channel in contact with an electrolyte (biological medium) whose potential is modulated by a gate electrode. The operation of an OECT relies on the penetration of ions of the electrolyte into the channel and their ability to change the doping state, and therefore the conductivity, of the channel. The identifying characteristic of these devices is that the interaction of ions with the channel spans the bulk of the organic electronic channel, which leads to a large amplification of the gate modulation (*6*). OECTs have therefore been integrated in a variety of biochemical sensing platforms, including implantable arrays, which record signals from electrically active cells with record-high sensitivities (*7*), or in vitro platforms, which measure metabolite concentrations in physiological fluids (*8*–*10*). Hence, OECTs directly interfacing with cell cultures were shown to assess the integrity and health of barrier-forming (non-electrogenic) cells with a degree of superiority over the traditional electrochemical impedance sensing platforms using electrodes (*11*). In these measurements, cells growing on the channel impede the ionic flux between the electrolyte and the channel and alter the performance of the device. While the first reported OECTs were based on polypyrrole (*12*), the workhorse material used typically as the channel is the conducting polymer poly(3,4-ethylenedioxythiophene) doped with poly(styrene sulfonate) (PEDOT:PSS) due to its notable stability in its oxidized and reduced forms. Especially important for cell-based applications, its optical transparency and its amenability to surface functionalization allow parallel optical and electrical assessment of cells (*13*) as well as controlled cell attachment and growth on its surface (*14*).

While most biological transducers incorporate [two-dimensional (2D)] monolayers of cells cultured on planar substrates, there is a growing recognition that data gleaned from flat biology approaches can be misleading. 3D approaches to cell culture are now widespread and are being embraced by the organ-on-chip community for human-relevant drug discovery and toxicology assays (*15*–*17*). Hence, a large variety of 3D models that better mimic in vivo physiology has been developed, including spheroids, organoids, and scaffolds, with the latter typically being a porous cell support matrix composed of synthetic materials or biopolymers (*18*, *19*). Integration of these complex systems with electrical transducers has been limited to flat electrodes (*20*–*23*), not compatible with intimate monitoring of the function of these complex models in a precise manner. However, as recently demonstrated, the ability of conducting polymers to be fabricated into mechanically soft hydrogels and

[1]Department of Chemical Engineering and Biotechnology, University of Cambridge, Philippa Fawcett Drive, Cambridge CB3 0AS, UK. [2]Department of Bioelectronics, Ecole Nationale Supérieure des Mines, CMP-EMSE, Gardanne 13541, France. [3]Department of Materials Science and Engineering, University of Ioannina, GR-45110 Ioannina, Greece. [4]Biological and Environmental Science and Engineering, King Abdullah University of Science and Technology (KAUST), Thuwal 23955-6900, Kingdom of Saudi Arabia.
*Corresponding author. Email: rmo37@cam.ac.uk (R.M.O.); cp645@cam.ac.uk (C.P.)

scaffolds (*24*) opens up exciting new possibilities to integrate electrically conducting materials with 3D cell cultures (*25*–*27*). Previously, the integration of scaffolds into OECTs was shown, but the large size of the devices meant very slow speeds and low transconductance, and no cell monitoring was shown (*26*). We recently showed for the first time the use of PEDOT:PSS scaffolds to simultaneously host and monitor (via impedance) cocultures of mammalian cell growth within its porous architecture (*28*). We were inspired by tissue engineering approaches to grow cells in 3D on porous scaffolds with mechanical and biochemical cues enabling cell growth, but with the addition of electrical functionality owing to the conducting polymer. Such a 3D electrode device offers enhanced sensing capabilities; however, extracting the critical parameters from the complex impedance spectrum is rather challenging.

Continuing from this work, here, we show the use of 3D macroporous scaffolds in an OECT configuration for dynamic monitoring of cell culture growth. We demonstrate easy tuning of these scaffolds in terms of electrical, mechanical, and biochemical properties due to an in situ lyophilization process, which we have adapted to assemble scaffolds inside fluidic tubes. The tubular structure facilitates gas exchange and fresh medium delivery to the cells that are grown inside the scaffold, resembling to some degree blood vessels. We demonstrate that cells grow readily and form tissue-like architectures within the conducting polymer scaffold constituting the channel of the transistor. The tissue formation gradually modulates the electronic properties of the conducting polymer scaffold, as evidenced by changes in both the steady-state and transient characteristics of the device. Correlating the changes in the performance of the transistor to the adhesion and growth of cells over time, we extract useful information regarding the tissue formation. This label-free, in situ, dynamic, and "living" electronic tool illustrates the potential of these scaffolds for real-time monitoring of 3D cell culture and compatibility with use in long-term organ-on-chip platforms.

RESULTS

The most common and relatively facile technique to shape a polymer into a 3D structure is through freeze drying (known as lyophilization) (*29*, *30*). Using these processes, free-standing macroporous scaffolds can be prepared from aqueous solutions/dispersion of polymers with mechanical stability and porosity adjusted by the material composition and the processing conditions. Moreover, as the base material is in liquid form, it is feasible to regulate the dimensions of the resulting solidified structure by the mold in which it is cast. This offers unprecedented ease in fabrication as well as great versatility for designing platforms based on these 3D materials with macroscopic pores. In our previous work (*28*), a fluidic tubing was integrated with a relatively large PEDOT:PSS-based scaffold (using a cuvette as a mold) to promote homogeneous cell accumulation inside the scaffold as well as provide continuous perfusion of nutrients required for cell growth over several days (*31*, *32*). We have now inverted and miniaturized this concept and designed a 3D cell monitoring platform based on a tubular T-shaped arrangement with the source, drain, and gate electrodes embedded inside the fluidics. This geometry allows the integration of a 3D conducting channel (the 3D conducting polymer scaffold) within the tube, which simultaneously provides perfusion capability, with easy interfacing to standard fluidic systems. The fabrication route of the transistor-in-a-tube ("tubistor") and the device architecture are shown in Fig. 1, A and B, respectively. The two uniaxial ends of the device act as the inlet and outlet ports, while the central opening is used for the integration of the source-drain electrodes. The gate electrode (i.e., Pt mesh or Ag/AgCl wire) is installed in the extension of the tube close to the inlet port. The 3D channel of the tubistor consists of a porous PEDOT:PSS scaffold formed in situ by the freeze-drying process, as described elsewhere (*26*). Briefly, the process involves freezing the aqueous polymer solution at a controlled rate, followed by sublimation of the ice crystals under high-vacuum conditions. This leads to a porous matrix with high surface-to-volume ratio and an extensive 3D network of interconnected pores. A schematic representation of the morphological transition driven by the freeze-drying process is shown in fig. S1. The dimensions of the tubular scaffold produced are defined by the inner diameter of the tube, while its size can be adjusted by controlling the injected volume. The tubistor is gated through a liquid electrolyte that bridges the bulk of the polymeric scaffold and the gate electrode. Despite the considerably larger transistor geometry and the "bulky" morphology of PEDOT:PSS, the operation mechanism of the tubistor is identical to that of 2D OECTs (*5*, *6*, *33*). For OECTs, applying a bias at the gate electrode injects electrolyte ions into the channel, leading to a change in the redox state of the conducting polymer. In the case of PEDOT:PSS scaffolds, upon application of a positive gate bias, cations from the electrolyte are injected into the complex matrix (consisting of sulfonate anion and hole pairs) and the anions are compensated. This causes extraction of holes and a consequent decrease in the drain current (i.e., dedoping of PEDOT:PSS) (illustrated in Fig. 1B). The transfer and output characteristics of the tubistor show a decrease of the drain current with gate voltage, consistent with operation in depletion mode (Fig. 1, D and E). On the basis of the model proposed by Rivnay and co-workers, the transconductance of OECTs scales with the volumetric capacitance of the channel and is directly dependent on the geometrical characteristics (*6*, *34*). Considering that the volume of the PEDOT:PSS channel in the tubistor is several hundred times greater than that in typical spin-cast devices (*33*), high transconductance values and slow switching speeds are expected. Despite the large channel length (>500 μm), the transconductance of a typical tubistor was found to exceed values of 12 mS due to the large width and overall thickness. The switching performance of the transistors was investigated using pulsed voltages at the gate electrode (Fig. 1F). Fitting the drain current transient triggered by a voltage pulse at the gate, we estimated the response time (τ) of the transistors. Typically, tubistors yielded slow switching speeds, with exponential rise times often exceeding ~1.5 s. Moreover, an asymmetric behavior between dedoping regime (V_{GS} = 0.2 V) and current recovery (V_{GS} = 0 V) was observed (fig. S2). This variation is reflected in the ratio of the response time values of the two regimes $\tau_{rec}/\tau_{dedop,}$ which was found to be approximately 1.4. This result indicates that the recovery process (at V_{GS} = 0 V) is slower than the dedoping and can be attributed to the slower cation drift from the semiconductor bulk to the electrolyte due to ion trapping.

Considering the high surface-to-volume ratio of the scaffolds, we posit that the gating of the 3D porous transistors by the electrolyte is more challenging compared to planar OECTs. The choice of gate electrode is thus crucial, and a good balance must be found between biocompatibility and gating efficiency (*35*). For the characterization of the tubistors, a nonpolarizable electrode such as Ag/AgCl was used, as the voltage drop at the gate electrode/electrolyte is minimal. Despite the extensive use of Ag/AgCl in electrophysiology, it has been

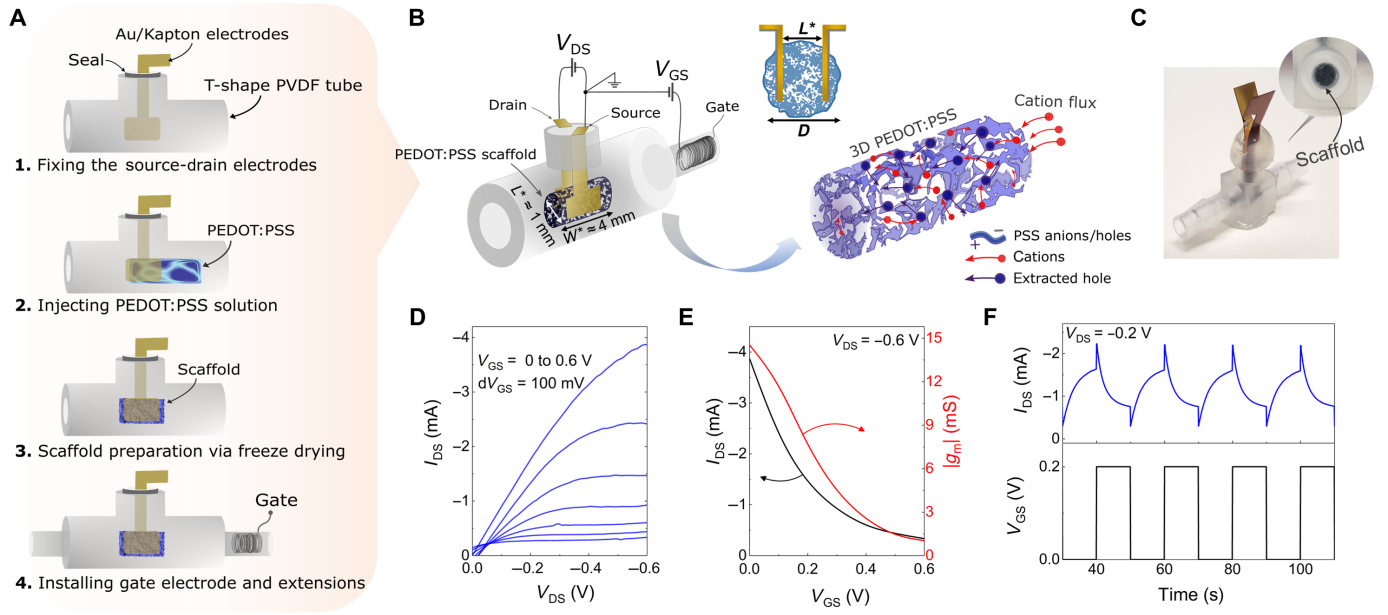

Fig. 1. Easy-to-fabricate 3D conducting polymer transistors in a tube: Tubistor. (**A**) Schematic representation of the fabrication process. (**B**) Schematic illustration of the device structure. The device is composed of three main parts: (i) a tubular cavity with three openings (two of these are for the contacts and the gate electrode and the other one is for perfusion), (ii) Au-coated flexible electrodes used as source (S) and drain (D) contacts of the channel fixed inside the tube, and (iii) a PEDOT:PSS scaffold as the channel with the gate electrode embedded inside the tube. To aid with visualization of the channel, a cross-sectional view shows how the electrodes are placed inside the scaffold. The schematic shows the dedoping process inside the channel as cations from the electrolyte are injected into the 3D PEDOT:PSS scaffold. (**C**) Photograph of a tubistor with a magnified image of the conducting scaffold inside the tube. Photo credit: Charalampos Pitsalidis. (**D**) Transistor output curves showing the drain current (I_{DS}) as a function of drain voltage (V_{DS}) for a gate voltage (V_{GS}) ranging from 0 to 0.6 V. (**E**) Transfer characteristics and the corresponding transconductance (g_m) of a typical tubistor at V_{DS} = −0.6 V. (**F**) Transient response of the tubistor to periodic square gate pulses (V_{GS} = 0.2 V for 10 s) at V_{DS} = −0.2 V. The electrolyte was a 0.1 M aqueous NaCl solution. The distance between the source-drain electrodes (L^*) in this specific device was approximately 1 mm, while the width (W^*) of the scaffold was 4 mm. The diameter (D) of the tubular scaffold was ~1.5 mm.

proven cytotoxic for long-term cell studies (*36*). An alternative strategy is the use of a high-capacitance gate electrode, such as PEDOT:PSS. We thus investigated the use of a secondary PEDOT:PSS scaffold as a gate electrode (fig. S3A). Regardless of the good gating provided in this case, electrical wiring and contacting of the gate scaffold inside the tube were found to be technically challenging. Pt electrodes show good biocompatibility; however, the gating efficiency is rather inefficient due to its polarizable character (fig. S3B). To overcome these limitations, we must substantially increase the surface of the gate electrode. As we show later in this work, a multiple folded Pt mesh electrode provides efficient gating (at the given channel geometry) for our 3D transistor as well as good cytocompatibility.

The morphological and structural properties of the scaffolds may have a great influence on the cell functionalities and the resulting tissue microenvironment. Specifically, the pore size and density represent the most important characteristics, as they affect the penetration of cells into the scaffold and define their spatial distribution within the 3D matrix (*37*). Moreover, they can affect the flow resistance, the transportation of nutrients, and the excretion of waste products. A simple way to control the pore morphology is by varying the cooling rate parameter. It has been previously reported that the pore size can be efficiently increased by decreasing the cooling rate (*38*). To validate this, we investigated the effect of various cooling rates (0.4, 0.8, and 1.2°C/min) on the pore morphology of PEDOT: PSS scaffolds with dodecylbenzenesulfonic acid (DBSA) as an additive (fig. S4A). The mean pore size [estimated from the scanning electron microscopy (SEM) images] showed a tendency to decrease with increased cooling rate from ~85.9 ± 15.0 to 47.9 ± 7.8. It should be noted that the cooling rate parameter is extracted by the shelf temperature values; thus, the actual cooling rate inside the tubing may be different. Despite the variations in the pore size, only slight fluctuations in the electrical performance of the corresponding devices were observed (fig. S4B). Subsequent experiments were carried out using the intermediate condition of cooling rate (0.8°C/min), as it gives sufficiently large pores and overall good uniformity.

Variations in the PEDOT:PSS formulation can also alter the electrical and mechanical properties of the resulting scaffolds. As we have shown previously, adding DBSA or collagen in the PEDOT:PSS solution markedly changes the conductivity or the mechanical stiffness, respectively (*28*). Following this rationale, we proceeded to investigate the effects of different PEDOT:PSS formulations on the electrical performance of the tubistors illustrated in SEM micrographs of neat PEDOT:PSS, PEDOT:PSS/DBSA, PEDOT:PSS/DBSA/collagen, and PEDOT:PSS/DBSA/SWCNT (single-walled carbon nanotube) scaffolds (Fig. 2, A to D). The scaffolds exhibited highly interconnected porous networks, with pore sizes ranging from ~50 to 120 μm. Here, the freeze-drying parameters during the fabrication of the various scaffolds were kept constant (T_C = −50°C, 0.8°C/min). In the case of neat PEDOT:PSS, a more random pore size distribution is apparent, while the inclusion of DBSA improves the homogeneity of pore formation likely due to its surfactant properties, which promote the dispersion of solid parts in the pristine solution.

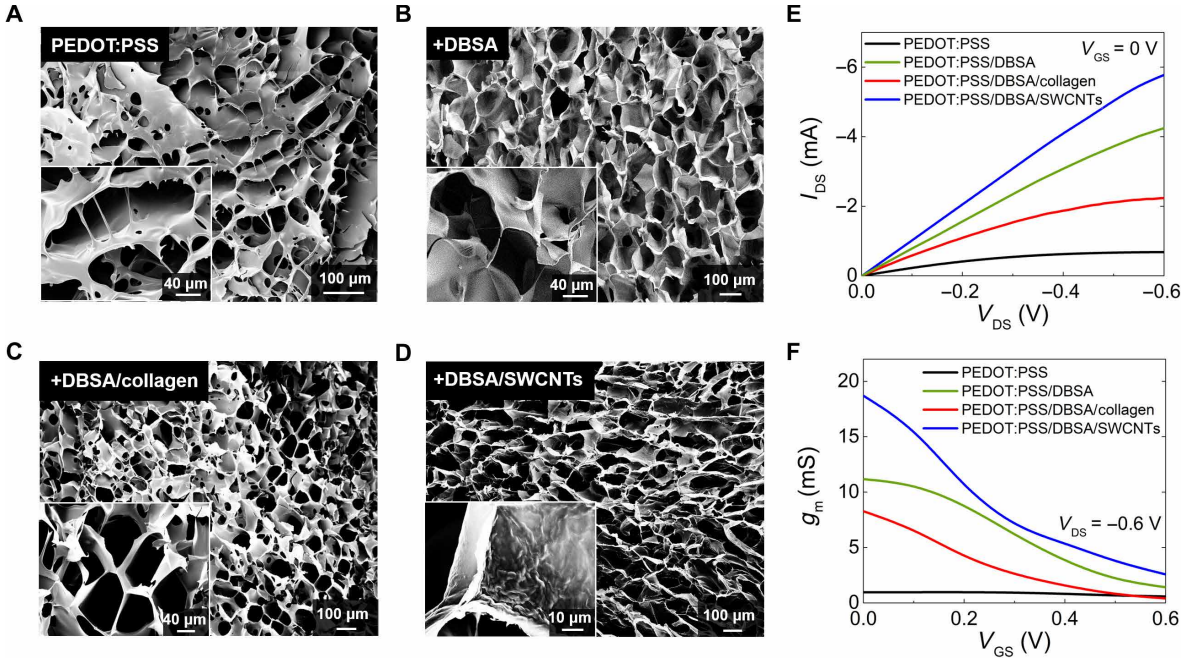

Fig. 2. Morphological and electrical characterization of various conducting scaffolds. SEM images of the tubistors based on (**A**) neat PEDOT:PSS, (**B**) PEDOT:PSS/DBSA, (**C**) PEDOT:PSS/DBSA/collagen, and (**D**) PEDOT:PSS/DBSA/SWCNT scaffolds. The insets show SEM images of the pores at higher magnification. (**E**) Comparative output transistor characteristics (at V_{GS} = 0 V) and (**F**) corresponding transconductance curves for the various types of scaffolds. The transistor characteristics are measured in phosphate-buffered saline (PBS) solution using a Ag/AgCl pellet as the gate electrode. The distance (*L**) between the source-drain electrodes was measured to be approximately 1 mm, while the width (*W**) of the scaffold in this case was 4 mm. Results shown are from representative devices.

The presence of collagen in the PEDOT:PSS/DBSA mixture did not seem to induce any macroscale morphological effect on the resulting porous structure. In the case of the SWCNT mixture, wire-like nanodomains protrude slightly from the scaffold surface (Fig. 2D, inset).

More quantifiable changes can be observed in the electrical behavior of the tubistors, namely, the comparative output characteristics and the evolution of transconductance at the given V_{GS} range (Fig. 2, E and F). When used as the channel material, DBSA-based scaffolds exhibited substantial improvement in the electrical performance compared to pristine samples, as confirmed by the transistor characteristics of the corresponding tubistors, consistent with previous reports on DBSA-enhanced conductivity of PEDOT:PSS (*25*, *39*). Specifically, the magnitude of I_{DS} increased about six times with DBSA (from ~0.7 to ~4.2 mA), while the g_m increased from 0.95 to 11.2 mS. Although the addition of collagen may provide better biocompatibility and mechanical properties for tissue growth studies, its insulating nature degrades the conductivity of the scaffolds and the overall performance of the tubistors. In contrast, the incorporation of SWCNTs into the PEDOT:PSS/DBSA mixture resulted in tubistors with high transconductance values of 18.7 mS (best recorded performance) (*40*, *41*). Future work will include a more detailed study on the structural, morphological, and electrical properties of PEDOT:PSS/nanomaterial (CNTs, graphene, etc.) scaffolds.

As described by Jimison *et al.* (*42*), OECTs can be used for assessing and monitoring the integrity of barrier tissues. In a first attempt to operate a tubistor as an electrochemical transducer for biological events, two different cell lines were seeded on tubular-shaped (length, 4 mm; diameter, 1.5 mm) PEDOT:PSS scaffolds, namely, barrier-forming kidney epithelial cells (MDCKII) and telomerase-immortalized fibroblasts (TIFs). An image of various free-standing PEDOT:PSS scaffolds is shown in Fig. 3A. In this set of experiments, the cell seeding and growth stage took place inside an Eppendorf tube for 3 days. The tissue-containing scaffolds were then inserted inside the tubistor to investigate the effects of cell growth on the electrical performance of the tubistor (Fig. 3B). Fluorescence images (Fig. 3, C and D) taken after 3 days of culture provide evidence of cell accumulation in the scaffold, with somewhat inhomogeneous cell distribution and coverage apparent for both cell types. This is consistent with previous observations of cell growth in PEDOT:PSS scaffolds and can be attributed to the lack of a perfusion system (*28*). While TIF cells appeared to be spread over the scaffold forming individual cell domains, scaffolds seeded with MDCKII cells exhibited high confluency, with tissue-like morphology at the pore surface, as shown in the magnified image of Fig. 3C.

The adhesion of cells and subsequent tissue formation inside the pores of the scaffold were seen to substantially change the drain current, as shown in the output characteristics of fig. S5. This change is accompanied with a shift toward negative V_{DS}, likely due to non-ideal physical contact between electrodes and semiconductor, which results in poor charge injection, especially in the cell-covered scaffolds. The growth of cells in the scaffolds was further found to affect the efficiency of the ionic signal transduction, expressed by the magnitude of g_m. Comparing the maximum normalized g_m values as a function of V_{GS} between the scaffolds containing cells and those without cells, we noticed a decrease of 72 and 60% for MDCKII cell–seeded (Fig. 3E) and TIF cell–seeded (Fig. 3F) scaffolds, respectively. In agreement with previous observations on planar OECTs, the formation of barrier tissue (e.g., MDCKII) on the PEDOT:PSS channel of the OECT changes the transistor performance, i.e., increase

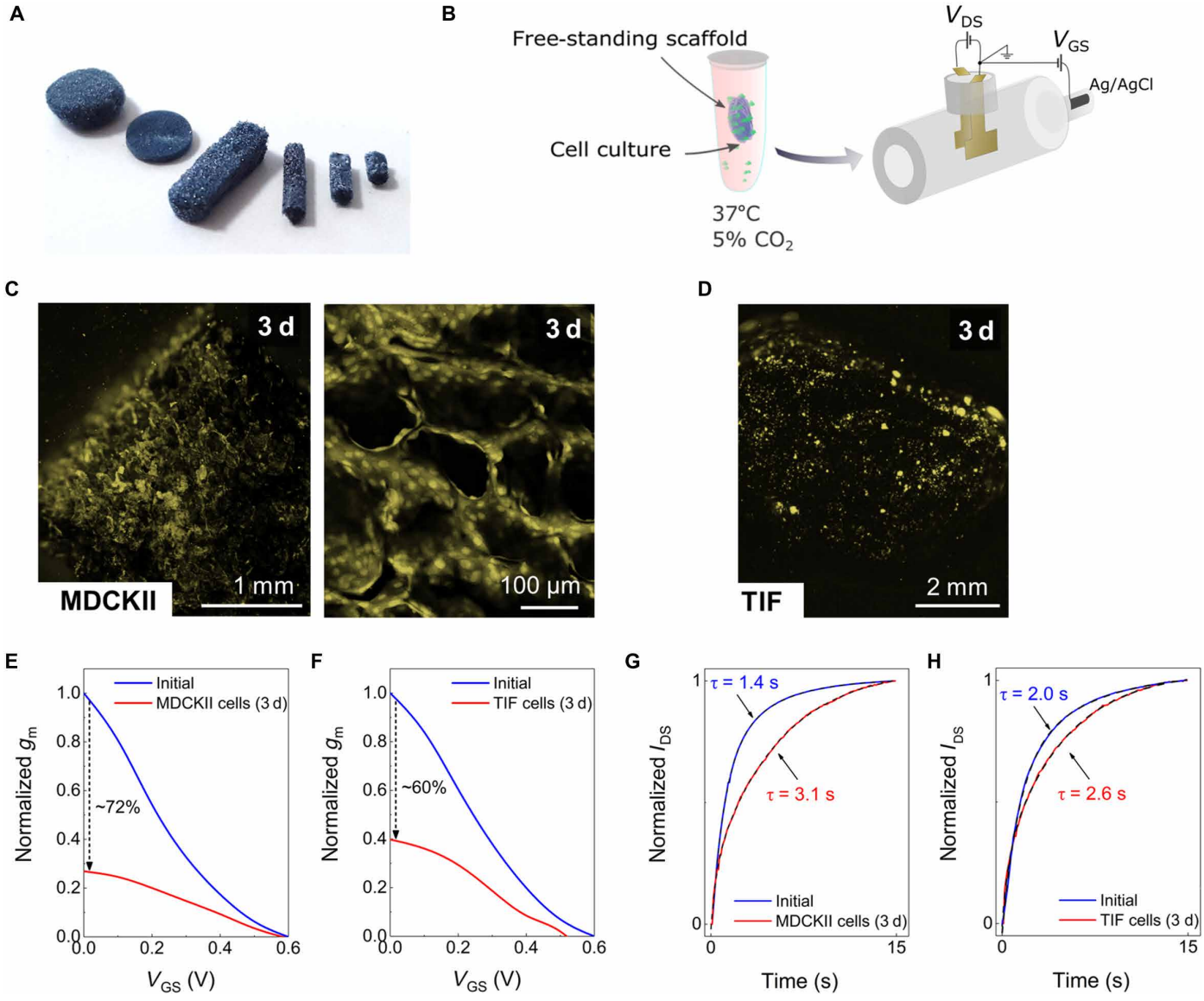

Fig. 3. Electronic monitoring of ex situ grown 3D cell cultures using tubistor. (**A**) Photograph of free-standing PEDOT:PSS scaffolds of various sizes and shapes. Photo credit: Charalampos Pitsalidis. (**B**) Sketch of the ex situ 3D cell growth and measurement process. Before the electrical measurements, the scaffold was placed in contact with the source-drain electrodes in the presence of culture medium. Fluorescence microscopy image PEDOT:PSS scaffolds seeded with (**C**) MDCKII and (**D**) TIF cells after 3 days of cell culture inside an Eppendorf tube. Scanned images were pseudo-colored yellow. Normalized transconductance (g_m) versus V_{GS} at V_{DS} = −0.6 V before and after culture with (**E**) MDCKII and (**F**) TIF cells. Normalized current response of the OECT to periodic square V_{GS} pulses with and without (**G**) MDCKII and (**H**) TIF cells. The dashed black line is the exponential fit used to extract the τ values. The electrical measurements were carried out using a Ag/AgCl gate electrode. The distance (*L**) between the source-drain electrodes was measured to be approximately 1.5 mm, while the width (*W**) of the scaffold in this set of experiments was 4 mm.

in response time (τ). This was further confirmed by the pulse characteristics of the tubistors (Fig. 3, G and H). A marked difference in the relative change of the response time between the two cell types can be observed. Specifically, in the case of the MDCKII epithelial cells where ionic transport is hindered by the tight barrier properties, the response time (τ) was found to increase substantially from 1.4 to 3.1 s. In contrast, the TIF cell (non–barrier tissue–forming cell)–seeded devices exhibited a negligible change from 2.0 to 2.6 s. We posit that this difference is due to additional resistance effects conveyed by the epithelial cells, in contrast to the fibroblast cells. This is supported by previous work screening multiple cell types (barrier-forming versus non–barrier-forming) on 2D planar devices (*43*). Control experiments carried out without cells in culture medium for 4 days showed only a slight degradation of the device performance, as shown in fig. S6. Specifically, a decrease in the I_{DS} of about 17% was measured, while the corresponding change in the maximum g_m was found to be approximately 18%.

To assess the versatility of our 3D devices, we performed in situ real-time monitoring of cell growth. The fluidic structure of the tubistors promotes the efficient perfusion of the scaffolds by supplying a continuous flow of medium (0.5 µl/min) during cell culture while monitoring the transistor parameters. As discussed earlier, to

render the tubistor biocompatible with long-term electrical measurements, a Pt mesh embedded inside the tubing was used as the gate electrode. A schematic illustration of the experimental setup is shown in Fig. 4A. In this set of experiments, MDCKII cells were cultured inside the tubistor without any pretreatment of the scaffold and imaged after 1 and 2 days (Fig. 4, B and C). A homogeneous spreading and distribution of cells is clearly visible throughout the scaffold, along with extensive tissue formation after 2 days of culture. This observation highlights the important role of a perfusion system when hosting 3D cell cultures. During these 2 days, we could monitor fluctuations in the electrical performance of the devices associated with various cellular growth stages. The output characteristics of the tubistors at certain time points during the cell culture process show a marked drop in the magnitude of I_{DS} (V_{DS} = −0.6 V) from −1.6 to 0.46 mA after the seeding and during the incubation (1 hour without flow), accompanied with a reduction of the g_m by more than two orders of magnitude (Fig. 4, D and E). We attribute these changes to the high density of the initial cell suspension, which may hamper the injection of charge carriers and the diffusion of ions. After the incubation step, the nonadherent cells were expelled by flowing fresh medium into the system, resulting in a partial recovery of the device performance. Additional experiments were carried out to investigate the initial effect of cell density on the device performance by varying the number of cells seeded into the scaffolds (4×10^3 versus 4×10^5 cells). We could observe a notable difference on the device performance after 1 hour of seeding with the different cell densities. The higher cell density seeded device resulted in a larger decrease in the current magnitude accompanied by a change in the g_m value of ~28% versus a ~16% change for the lower cell density (fig. S7). The growth of cells in the 3D matrix has a direct effect on the device performance, most likely related to the ionic and channel resistance. Thus, by adjusting the cell number at a given scaffold size, we can tune the sensitivity level of the device to assess the initial stages of cell attachment. During this stage, device-to-device variations may be observed due to the random cell distribution and coverage. Notably, after cell attachment, the devices show a steady behavior, while a gradual decrease over time in the g_m magnitude was observed after t = ~16 hours of cell culture, as shown in Fig. 4E. The cellular organization inside the scaffolds during the first 48 hours strongly dictates the electrical operation of the devices, with a relative decrease in the maximum g_m value of approximately 82%. Because of the small size of the scaffold and the good perfusion capability of the tubistor, we were able to obtain extensive cell growth after only 2 days of culture. After 44 hours of cell culture, there are no major variations in the g_m, indicating that a confluent tissue has been obtained. In situ electrical measurements of an incubated device without cells did not show any significant variation in the g_m value over time, as shown in the control curve (denoted as stars) of Fig. 4E.

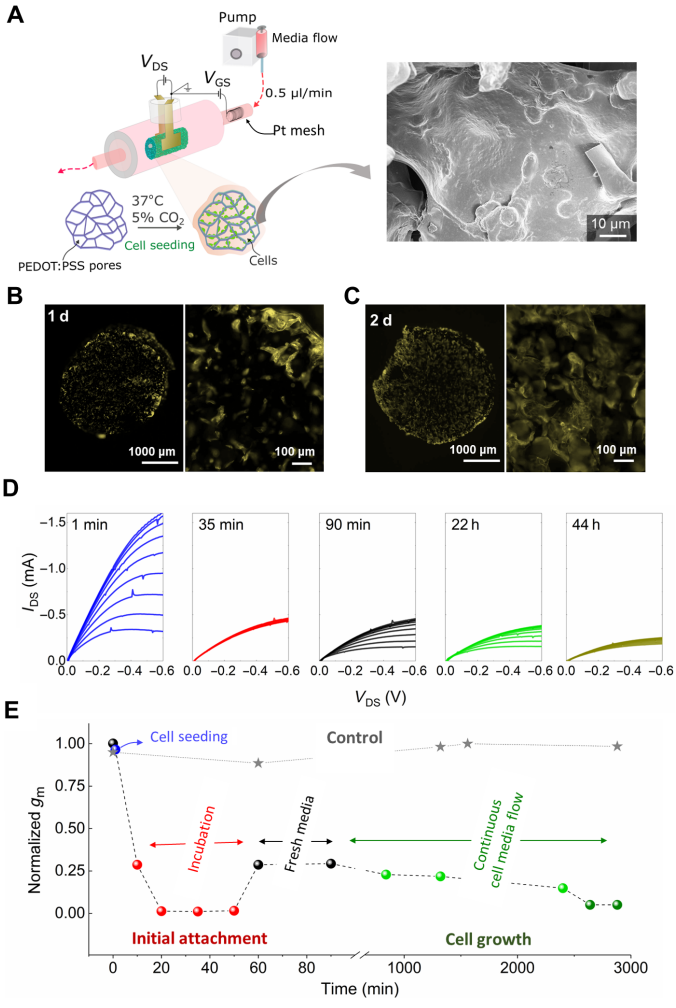

Fig. 4. Tubistors are compatible with in situ monitoring of cells. (**A**) Illustration of the experimental setup used in the dynamic experiments. SEM image showing the MDCKII cells cultured in situ in the PEDOT:PSS scaffold for ~2 days, providing evidence that the cells were able to adhere and form tissue inside the tubistor. The gray line (star points) shows the evolution of transconductance over time of a cell-free device incubated (37°C, 5% CO_2) in cell culture medium. Fluorescence images of MDCKII cells cultured in situ for (**B**) 1 day and (**C**) 2 days. Scanned images were pseudo-colored yellow. (**D**) Representative in situ output characteristics of the tubistors recorded during cell growth at various time points. (**E**) Corresponding evolution of normalized transconductance values at different stages of cell culture process. The electrical measurements were carried out using Pt mesh gate electrode embedded inside the tube extension. The device was connected to an electrical measuring unit during cell culture.

We and others have shown that cell adhesion can greatly change the impedance of electrodes on which they are cultured; however, other processes such as barrier formation (typical of epithelial cells such as the MDCKII cells used here) can have additional electrical effects that may be observed. To illustrate the future potential of these devices for continuous toxicology monitoring, we performed preliminary experiments with EGTA, a calcium chelator that disrupts paracellular junctions, thus impairing the tissue barrier. Confirming the effects of EGTA (100 mM) on our 3D cultured devices, a progressive disruption of the cell barrier was evidenced by a decrease in the time constant τ, as the tight junctions undergo disassembly (fig. S8A). Specifically, a rapid decrease in the normalized τ value was observed within the first 15 min, implying compromise of the barrier integrity (fig. S8B). These findings are in good agreement with our previous studies on the effects of EGTA on paracellular permeability using 2D OECTs (*13*, *44*).

DISCUSSION

From the first demonstration of the recording of a leech neuron using Si-based transistor technology (*4*) to more recent studies such as probing single-cell activity using a tunable 3D sensing nanoscale

field-effect transistor by Tian *et al.* (*45*), transistors have proven highly advantageous for cell monitoring. As inherently more biomimetic transistors, due to the organic nature of the material comprising the channel, OECTs have gone from strength to strength in interfacing with cells. In particular, OECTs have been used not only for electroactive cell monitoring but also for monitoring of tissue integrity, with a degree of superiority over the traditional two-electrode format used in electrical impedance sensing of cells (*11*, *46*). Apart from the patch clamp technique (or microneedle-type approaches) to monitor intracellular electrical activity, electrodes for interfacing with cells are themselves almost exclusively 2D, limiting efficiency in electrical measurements of more physiologically relevant 3D tissue structures. Undeniably, 3D cell biology has and will continue to benefit from developments in materials science and biology with sophisticated and physiologically relevant complex models, and so technologies that can adapt to accurately monitor those systems are urgently needed. Hence, our innovative concept of a fully integrated 3D polymer-based transistor in a tube as both the cell tissue support and the active transducer heralds a new path toward truly biomimetic 3D in vitro (bio)electronics. We have successfully addressed challenges from a (micro)electronics standpoint related to stability, electrical performance, and system integration. Our 3D OECT was shown to exhibit remarkably good and temporally stable electrical characteristics and robustness, owing to its design and the in situ formation of the conducting channel. From a materials/functionality standpoint, we have shown the potential to fabricate a wide variety of mesoscale and macroscale geometries, and that by tuning the components in the precursor conducting solution, we can easily adjust both the device performance (i.e., electrical conductivity) and the scaffold properties (i.e., porosity) to fit different purposes. We also found that our devices exhibited stress-dependent electrical behavior owing to the good elastic properties of the PEDOT:PSS scaffolds, as shown in fig. S9. The cumulative compression of the scaffold inside the tubistor led to a gradual increase in the measured drain current possibly due to the establishment of more conducting points. Since this observation was beyond our current application scope, future studies will investigate more thoroughly the capability of our device for pressure sensing.

From a biological standpoint, we have shown excellent compatibility of the 3D conducting scaffolds with two different types of cells both when seeded ex situ and in situ using continuous flow through our integrated fluidic. The integrated fluidic provides greater ease of use and compatibility with biological systems. As expected, the in situ seeding resulted in substantially faster cell adhesion and growth due to the continuous exchange of medium through our perfusion system. The tubistor was also used as the active transducer of cell attachment and growth within the scaffold. As observed, different cell types resulted in different changes both in the steady state and in the transient response. As expected, the barrier-forming cells inhibited the ionic flow to a greater extent and resulted in a more pronounced suppression of the electrical characteristics when compared to cells that are not known to form ionic barriers. In situ dynamic measurements of the tubistor with the barrier-type tissue cells revealed useful information on the timescale of several events, allowing us to postulate the critical stages of cell attachment and growth using the transistor's gain as the figure of merit for biotransduction. Together, this work opens up a new unchartered area of integrated 3D bioelectronics toward more physiologically relevant in vitro systems. Our future vision includes the development of more complex organoid-type systems including multiple cell types in a compartmentalized manner to study the underlying mechanisms of diseases and aid toward the development of associated therapies.

MATERIALS AND METHODS

Preparation of the 3D scaffolds

Scaffolds were prepared from an aqueous dispersion of PEDOT:PSS (Clevios PH 1000, Heraeus) at a concentration of 1.25 wt %. To enhance the mechanical properties and the stability of the scaffolds in aqueous solution, (3-glycidoxypropyl)-trimethoxysilane (Sigma-Aldrich) was added as a crosslinker (3 wt %). Moreover, to enhance further the conductivity of the scaffolds, we added 0.5% DBSA (Sigma-Aldrich). This was the basic formulation used for the fabrication of the free-standing conducting scaffolds as well as for the tubistors used in the cell studies. Two different additives were used with the basic formulation to evaluate the effects on the electrical behavior of the scaffolds: (i) collagen (0.05 wt %, type I from rat tail) and (ii) SWCNTs (0.5 wt %). Before the freeze-drying process, the PEDOT:PSS dispersion was poured into various molds and tubing systems. For the fabrication of the tubistor, the volume injected inside the tube ranged between 40 and 80 μl depending on the desired dimensions of the system. The samples were then placed in a freeze dryer (Cryotec and Virtis AdVantage 2.0 BenchTop), where they were frozen from 5° to −50°C at a controlled cooling rate of −0.8°C min^{-1} (for the standard fabricated devices), at which point the ice phase was sublimed from the scaffolds, as described by Wan *et al.* (*26*). After the freeze-drying process, the samples were baked at 70°C for 2 hours. Before device electrical measurements and cell experiments, all scaffolds were rinsed with deionized (DI) water multiple times, and they were then kept in DI water for 24 hours to enable the diffusion of low molecular components out of the structure. For the cell culture experiments, the samples were sterilized using 70% ethanol for about 30 min.

Device preparation

T-shaped tubes (Cole Parmer) were used as hosting structures for the fabrication of the tubistors. For the fabrication of source and drain electrodes, Au-coated (150 nm) Kapton films (120 μm) were used. Using the top opening, the source-drain electrodes were fixed inside the tube using a temporary cylindrical separator to avoid any contact between the two electrodes. The distance between the source and drain electrodes varied from 0.5 to 1.5 mm. Medical glue was used to seal the top opening. Before injection of the PEDOT:PSS solution, the system was washed and dried under nitrogen to remove possible contaminants. Three different gate electrodes were tested with the tubistor devices: (i) Ag/AgCl, (ii) Pt, and (iii) PEDOT:PSS. The different gates were placed inside a tubing extension and sealed. For long-term cell monitoring experiments, we used a Pt mesh electrode. The size of the Pt electrode was substantially larger than the scaffold to ensure efficient gating.

Scaffold and device characterization

The microstructure and morphology of the scaffolds were performed using SEM. SEM ULTRA 55 (Carl Zeiss) was used to evaluate the invasion of cells into the scaffolds. Briefly, cells in the scaffold were fixed in 2.5% glutaraldehyde in 0.1 M cacodylate buffer overnight at 4°C. After extensive washing with PBS, the scaffold was then dehydrated in a graded ethanol series and dried using hexamethyldisilazane

solution. Last, the sample was coated with 15-nm gold/paladium and analyzed at 5-kV acceleration voltages. The electrical characterization was performed using a solution of 100 mM NaCl in DI water as the electrolyte. The transistor characteristics were measured using a Keithley 2612 source meter, a customized LabVIEW software, and a Keysight B1500A parameter analyzer. The experiments were carried out in ambient atmosphere when no cells were involved, while for the cell studies an incubator at a temperature of 37°C and CO_2 level of 5% was used.

For the estimation of the pore size, SEM image analysis was used. Average pore diameter was measured on the basis of $n = 40$ pores per scaffold.

Cell culture experiments

Two cell types were used for the experiments: canine epithelial kidney cells (MDCKII, a gift from F. Luton, Institut de Pharmacologie Moléculaire et Cellulaire, Valbonne) and human TIFs (a gift from E. Van Obberghen-Schilling, Institut de Biologie de Valrose). MDCKII cells were cultured in low-glucose Dulbecco's modified Eagle's medium (DMEM) supplemented with 10% fetal bovine serum, 2 mM glutamine, penicillin (50 U ml^{-1}), and streptomycin (50 μg ml^{-1}). Fibroblasts were cultured in high-glucose DMEM and supplemented as previously described without glutamine. Once cells were detached from the tissue culture flask using a solution of 0.25% trypsin, cell suspension was centrifuged and supernatant was replaced by fresh medium. The fresh cell suspension (100 μl) was mixed with 100 μl of 0.4% trypan blue. Cells were counted using a glass hemocytometer and resuspended to prepare the desired cell concentration. Before cell seeding, scaffolds were kept submerged in cell medium for 2 hours at 37°C, allowing protein adhesion.

For the free-standing scaffold experiment, the medium was completely removed from the scaffold by placing it onto an absorber for 2 min. Cell seeding was done right after by dipping the dried scaffold into a cell suspension (MDCKII or TIF; 5×10^6 cells/ml), allowing cell penetration by capillarity forces. Then, the scaffold was kept at 37°C for 1 hour, allowing cell attachment and spread before changing the medium to remove nonattached cells. Cell culture maintenance was done by placing the scaffold into an Eppendorf tube filled with the medium for up to 3 days.

For in situ experiments, the medium was not removed to prevent any bubble formation inside the device, so cells were directly injected into the scaffold using the fluidic tubing at a velocity of 1.5 μl/min. Cell culture maintenance was done using cell medium supplemented with 5 mM Hepes and a continuous flow rate of 0.5 μl/min for 2 days.

For the cell adhesion experiments, two different cell suspensions were prepared: 5×10^6 and 5×10^4 cells/ml. A volume of 80 μl was injected inside the scaffold device, resulting in 4×10^5 and 4×10^3 cells, respectively. The electrical measurements were carried out before cell seeding and after incubating the devices for 1 hour at 37°C.

Immunofluorescence staining

MDCKII and TIF cells were fixed in 4% paraformaldehyde for 20 min at room temperature. The scaffolds were washed extensively with PBS and incubated with rhodamine phalloidin (Sigma) for 30 min to label actin filament. Fluorescence images of the scaffolds were obtained using an epifluorescence/confocal microscope (Axio Observer Z1 LSM 800, Zeiss).

EGTA experiments

MDCKII cells were seeded inside the scaffold devices and incubated to grow for 3 days. After stabilization of the devices for several minutes, we recorded the electrical signal (transient current response) to investigate the effects of EGTA addition. Specifically, a 100 mM solution of EGTA was diluted in cell medium (Alfa Aesar EGTA 0.5 M aqueous solution, J60767) and injected into the scaffold through the fluidic circuit in a steady manner. The transistor recording was carried out for several minutes after EGTA injection. The following parameters were used during the transient response measurements: $V_{DS} = -0.3$ V, $V_{GS} = 0.3$ V, on time $t = 15$ s. Data analysis was performed to fit the time constant for each individual pulse (*13*). Control experiments were carried out by exposing a cell-free scaffold to the EGTA solution for a certain period of time, as shown in the normalized data of fig. S8C.

SUPPLEMENTARY MATERIALS

Supplementary material for this article is available at http://advances.sciencemag.org/cgi/content/full/4/10/eaat4253/DC1

Fig. S1. Freeze-drying process for the fabrication of PEDOT:PSS scaffolds.
Fig. S2. Transient response of the tubistor.
Fig. S3. Effect of gate electrode on the electrical performance of the tubistor.
Fig. S4. Effect of pore size on the electrical performance of the tubistor devices.
Fig. S5. Monitoring the effect of 3D cell cultures on the steady-state characteristics of the transistor.
Fig. S6. Long-term stability of the tubistor in the presence of cell culture medium.
Fig. S7. Monitoring the effects of cell density during the initial cell attachment stage.
Fig. S8. Effect of EGTA on the barrier function of cells cultured in the tubistor.
Fig. S9. Effect of the compression strain on the electrical properties of the tubistors.

REFERENCES AND NOTES

1. M. E. Spira, A. Hai, Multi-electrode array technologies for neuroscience and cardiology. *Nat. Nanotechnol.* **8**, 83–94 (2013).
2. F. Heer, W. Franks, A. Blau, S. Taschini, C. Ziegler, A. Hierlemann, H. Baltes, CMOS microelectrode array for the monitoring of electrogenic cells. *Biosens. Bioelectron.* **20**, 358–366 (2004).
3. I. Giaever, C. R. Keese, Monitoring fibroblast behavior in tissue culture with an applied electric field. *Proc. Natl. Acad. Sci. U.S.A.* **81**, 3761–3764 (1984).
4. P. Fromherz, A. Offenhäusser, T. Vetter, J. Weis, A neuron-silicon junction: A Retzius cell of the leech on an insulated-gate field-effect transistor. *Science* **252**, 1290–1293 (1991).
5. J. Rivnay, S. Inal, A. Salleo, R. M. Owens, M. Berggren, G. G. Malliaras, Organic electrochemical transistors. *Nat. Rev. Mater.* **3**, 17086 (2018).
6. J. Rivnay, P. Leleux, M. Ferro, M. Sessolo, A. Williamson, D. A. Koutsouras, D. Khodagholy, M. Ramuz, X. Strakosas, R. M. Owens, C. Benar, J.-M. Badier, C. Bernard, G. G. Malliaras, High-performance transistors for bioelectronics through tuning of channel thickness. *Sci. Adv.* **1**, e1400251 (2015).
7. D. Khodagholy, T. Doublet, P. Quilichini, M. Gurfinkel, P. Leleux, A. Ghestem, E. Ismailova, T. Hervé, S. Sanaur, C. Bernard, G. G. Malliaras, In vivo recordings of brain activity using organic transistors. *Nat. Commun.* **4**, 1575 (2013).
8. A.-M. Pappa, O. Parlak, G. Scheiblin, P. Mailley, A. Salleo, R. M. Owens, Organic electronics for Point-of-Care metabolite monitoring. *Trends Biotechnol.* **36**, 45–59 (2018).
9. X. Ji, H. Yuen Lau, X. Ren, B. Peng, P. Zhai, S. P. Feng, P. K. L. Chan, Highly sensitive metabolite biosensor based on organic electrochemical transistor integrated with microfluidic channel and poly(n-vinyl-2-pyrrolidone)-capped platinum nanoparticles. *Adv. Mater. Technol.* **1**, 1600042 (2016).
10. A. M. Pappa, S. Inal, K. Roy, Y. Zhang, C. Pitsalidis, A. Hama, J. Pas, G. G. Malliaras, R. M. Owens, Polyelectrolyte layer-by-layer assembly on organic electrochemical transistors. *ACS Appl. Mater. Interfaces* **9**, 10427–10434 (2017).
11. J. Rivnay, M. Ramuz, P. Leleux, A. Hama, M. Huerta, R. M. Owens, Organic electrochemical transistors for cell-based impedance sensing. *Appl. Phys. Lett.* **106**, 043301 (2015).
12. H. S. White, G. P. Kittlesen, M. S. Wrighton, Chemical derivatization of an array of three gold microelectrodes with polypyrrole: Fabrication of a molecule-based transistor. *J. Am. Chem. Soc.* **106**, 5375–5377 (1984).
13. M. Ramuz, A. Hama, M. Huerta, J. Rivnay, P. Leleux, R. M. Owens, Combined optical and electronic sensing of epithelial cells using planar organic transistors. *Adv. Mater.* **26**, 7083–7090 (2014).

14. D. Ohayon, C. Pitsalidis, A. M. Pappa, A. Hama, Y. Zhang, L. Gallais, R. M. Owens, Laser patterning of self-assembled monolayers on PEDOT:PSS films for controlled cell adhesion. *Adv. Mater. Interfaces* **4**, 1700191 (2017).
15. I. Maschmeyer, A. K. Lorenz, K. Schimek, T. Hasenberg, A. P. Ramme, J. Hübner, M. Lindner, C. Drewell, S. Bauer, A. Thomas, N. S. Sambo, F. Sonntag, R. Lauster, U. Marx, A four-organ-chip for interconnected long-term co-culture of human intestine, liver, skin and kidney equivalents. *Lab Chip* **15**, 2688–2699 (2015).
16. E.-M. Materne, A. P. Ramme, A. P. Terrasso, M. Serra, P. M. Alves, C. Brito, D. A. Sakharov, A. G. Tonevitsky, R. Lauster, U. Marx, A multi-organ chip co-culture of neurospheres and liver equivalents for long-term substance testing. *J. Biotechnol.* **205**, 36–46 (2015).
17. A. Roth, T. Singer, The application of 3D cell models to support drug safety assessment: Opportunities & challenges. *Adv. Drug Deliv. Rev.* **69**, 179–189 (2014).
18. B. M. Baker, C. S. Chen, Deconstructing the third dimension: How 3D culture microenvironments alter cellular cues. *J. Cell Sci.* **125**, 3015–3024 (2012).
19. F. J. O'Brien, Biomaterials & scaffolds for tissue engineering. *Mater. Today* **14**, 88–95 (2011).
20. D. Seidel, J. Obendorf, B. Englich, H.-G. Jahnke, V. Semkova, S. Haupt, M. Girard, M. Peschanski, O. Brüstle, A. A. Robitzki, Impedimetric real-time monitoring of neural pluripotent stem cell differentiation process on microelectrode arrays. *Biosens. Bioelectron.* **86**, 277–286 (2016).
21. M. Huerta, J. Rivnay, M. Ramuz, A. Hama, R. M. Owens, Research update: Electrical monitoring of cysts using organic electrochemical transistors. *APL Mater.* **3**, 030701 (2015).
22. V. Curto, M. Ferro, F. Mariani, E. Scavetta, R. Owens, A planar impedance sensor for 3D spheroids. *Lab Chip* **18**, 933–943 (2018).
23. J. Pas, C. Pitsalidis, D. A. Koutsouras, P. P. Quilichini, F. Santoro, B. Cui, L. Gallais, R. P. O'Connor, G. G. Malliaras, R. M. Owens, Neurospheres on patterned PEDOT:PSS microelectrode arrays enhance electrophysiology recordings. *Adv. Biosyst.* **2**, 1700164 (2018).
24. R. Balint, N. J. Cassidy, S. H. Cartmell, Conductive polymers: Towards a smart biomaterial for tissue engineering. *Acta Biomater.* **10**, 2341–2353 (2014).
25. A. G. Guex, J. L. Puetzer, A. Armgarth, E. Littmann, E. Stavrinidou, E. P. Giannelis, G. G. Malliaras, M. M. Stevens, Highly porous scaffolds of PEDOT:PSS for bone tissue engineering. *Acta Biomater.* **62**, 91–101 (2017).
26. A. M.-D. Wan, S. Inal, T. Williams, K. Wang, P. Leleux, L. Estevez, E. P. Giannelis, C. Fischbach, G. G. Malliaras, D. Gourdon, 3D conducting polymer platforms for electrical control of protein conformation and cellular functions. *J. Mater. Chem. B* **3**, 5040–5048 (2015).
27. D. Iandolo, A. Ravichandran, X. Liu, F. Wen, J. K. Y. Chan, M. Berggren, S.-H. Teoh, D. T. Simon, Development and characterization of organic electronic scaffolds for bone tissue engineering. *Adv. Healthc. Mater.* **5**, 1505–1512 (2016).
28. S. Inal, A. Hama, M. Ferro, C. Pitsalidis, J. Oziat, D. Iandolo, A. M. Pappa, M. Hadida, M. Huerta, D. Marchat, P. Mailley, R. M. Owens, Conducting polymer scaffolds for hosting and monitoring 3D cell culture. *Adv. Biosyst.* **1**, 1700052 (2017).
29. T. Lu, Y. Li, T. Chen, Techniques for fabrication and construction of three-dimensional scaffolds for tissue engineering. *Int. J. Nanomed.* **8**, 337–350 (2013).
30. N. Annabi, J. W. Nichol, X. Zhong, C. Ji, S. Koshy, A. Khademhosseini, F. Dehghani, Controlling the porosity and microarchitecture of hydrogels for tissue engineering. *Tissue Eng. Part B Rev.* **16**, 371–383 (2010).
31. A. C. Urbaczek, P. A. G. C. Leão, F. Z. R. de Souza, A. Afonso, J. Vieira Alberice, L. T. D. Cappelini, I. Z. Carlos, E. Carrilho, Endothelial cell culture under perfusion on a polyester-toner microfluidic device. *Sci. Rep.* **7**, 10466 (2017).
32. F. Yu, R. Deng, W. H. Tong, L. Huan, N. Chan Way, A. IslamBadhan, C. Iliescu, H. Yu, A perfusion incubator liver chip for 3D cell culture with application on chronic hepatotoxicity testing. *Sci. Rep.* **7**, 14528 (2017).
33. D. Khodagholy, J. Rivnay, M. Sessolo, M. Gurfinkel, P. Leleux, L. H. Jimison, E. Stavrinidou, T. Herve, S. Sanaur, R. M. Owens, G. G. Malliaras, High transconductance organic electrochemical transistors. *Nat. Commun.* **4**, 2133 (2013).
34. C. M. Proctor, J. Rivnay, G. G. Malliaras, Understanding volumetric capacitance in conducting polymers. *J. Polym. Sci. Part B Polym. Phys.* **54**, 1433–1436 (2016).
35. M. Ramuz, K. Margita, A. Hama, P. Leleux, J. Rivnay, I. Bazin, R. M. Owens, Optimization of a planar all-polymer transistor for characterization of barrier tissue. *ChemPhysChem* **16**, 1210–1216 (2015).
36. W. F. Jackson, B. R. Duling, Toxic effects of silver-silver chloride electrodes on vascular smooth muscle. *Circ. Res.* **53**, 105–108 (1983).
37. F. P. W. Melchels, B. Tonnarelli, A. L. Olivares, I. Martin, D. Lacroix, J. Feijen, D. J. Wendt, D. W. Grijpma, The influence of the scaffold design on the distribution of adhering cells after perfusion cell seeding. *Biomaterials* **32**, 2878–2884 (2011).
38. F. J. O'Brien, B. A. Harley, I. V. Yannas, L. Gibson, Influence of freezing rate on pore structure in freeze-dried collagen-GAG scaffolds. *Biomaterials* **25**, 1077–1086 (2004).
39. Y.-J. Lin, W.-S. Ni, J.-Y. Lee, Effect of incorporation of ethylene glycol into PEDOT:PSS on electron phonon coupling and conductivity. *J. Appl. Phys.* **117**, 215501 (2015).
40. S. Inal, G. G. Malliaras, J. Rivnay, Benchmarking organic mixed conductors for transistors. *Nat. Commun.* **8**, 1767 (2017).
41. A. Malti, J. Edberg, H. Granberg, Z. U. Khan, J. W. Andreasen, X. Liu, D. Zhao, H. Zhang, Y. Yao, J. W. Brill, I. Engquist, M. Fahlman, L. Wågberg, X. Crispin, M. Berggren, An organic mixed ion-electron conductor for power electronics. *Adv. Sci.* **3**, 1500305 (2015).
42. L. H. Jimison, S. A. Tria, D. Khodagholy, M. Gurfinkel, E. Lanzarini, A. Hama, G. G. Malliaras, R. M. Owens, Measurement of barrier tissue integrity with an organic electrochemical transistor. *Adv. Mater.* **24**, 5919–5923 (2012).
43. M. Ramuz, A. Hama, J. Rivnay, P. Leleux, R. M. Owens, Monitoring of cell layer coverage and differentiation with the organic electrochemical transistor. *J. Mater. Chem. B* **3**, 5971–5977 (2015).
44. S. Tria, L. H. Jimison, A. Hama, M. Bongo, R. M. Owens, Sensing of EGTA mediated barrier tissue disruption with an organic transistor. *Biosensors* **3**, 44–57 (2013).
45. B. Tian, T. Cohen-Karni, Q. Qing, X. Duan, P. Xie, C. M. Lieber, Three-dimensional, flexible nanoscale field-effect transistors as localized bioprobes. *Science* **329**, 830–834 (2010).
46. J. Rivnay, P. Leleux, A. Hama, M. Ramuz, M. Huerta, G. G. Malliaras, R. M. Owens, Using white noise to gate organic transistors for dynamic monitoring of cultured cell layers. *Sci. Rep.* **5**, 11613 (2015).

Acknowledgments

Funding: We acknowledge funding from the ANR 3Bs project (ANR15-CE18-0004-001 to S.I. and C.P.) and a bourse doctorale from Ecole des Mines de St. Etienne (to M.P.F.). Additional funding was provided by an H2020 ERC CoG grant "IMBIBE" GA No. 723951 (to R.M.O. and C.P.) and an H2020-MSCA-IF-2015 grant "SMART-BONE" GA No. 704175 (to D.I.). **Author contributions:** C.P. conceived, executed, and analyzed results of experiments. M.P.F. did cell culture and SEM. D.I. aided with SEM and scaffold characterization. L.T. prepared and characterized SWCNTs. S.I. aided with initial concept and tubistor preparation. R.M.O. conceived and directed research on the paper. The manuscript was written and edited by C.P. and R.M.O. **Competing interests:** C.P., S.I., and R.M.O. are inventors on a patent related to this work filed with the French patent authority (application no. FR 1758683, submitted on 20 September 2017). All other authors declare that they have no competing interests. **Data and materials availability:** All data needed to evaluate the conclusions in the paper are present in the paper and/or the Supplementary Materials. Additional data related to this paper may be requested from the authors.

Submitted 25 February 2018
Accepted 19 September 2018
Published 26 October 2018
10.1126/sciadv.aat4253

Citation: C. Pitsalidis, M. P. Ferro, D. Iandolo, L. Tzounis, S. Inal, R. M. Owens, Transistor in a tube: A route to three-dimensional bioelectronics. *Sci. Adv.* **4**, eaat4253 (2018).